Evaluating the potential capability of Selenium nanoparticles on degradation of hazardess textile dye using environmental friendly approach

Haewon Byeon[1], V. Puvana Devi[2], A. Murugan[3], Anu Tonk[4], K. Haribabu[5], Harshal Patil[6] and V.G. Anisha Gnana Vincy[7]

[1]Department of AI-Big Data, College of AI Convergence, Inje University, Gimhae, 50834, Republic of Korea.

[2]Assistant Professor, Department of Chemistry, Government Arts and Science College, Avinashi, Tamil Nadu, India.

[3]Professor, Department of Mechanical Engineering, Rajiv Gandhi College of Engineering and Technology, Puducherry, India.

[4]Assistant Professor-Sr Scale, Department of Multidisciplinary Engineering, The NorthCap University, Gurugram, India.

[5]Associate Professor, Department of Mechanical Engineering, SCAD College of Engineering and Technology, Cheranmahadevi, Tamil Nadu, India.

[6]Associate Professor, Department of Computer Science and Engineering, Symbiosis Institute of Technology, Symbiosis International (Deemed University), Pune, India.

[7]Assistant Professor, Dhaanish Ahmed College of Engineering, Chennai, Tamil Nadu, India.

GRAPHICAL ABSTRACT
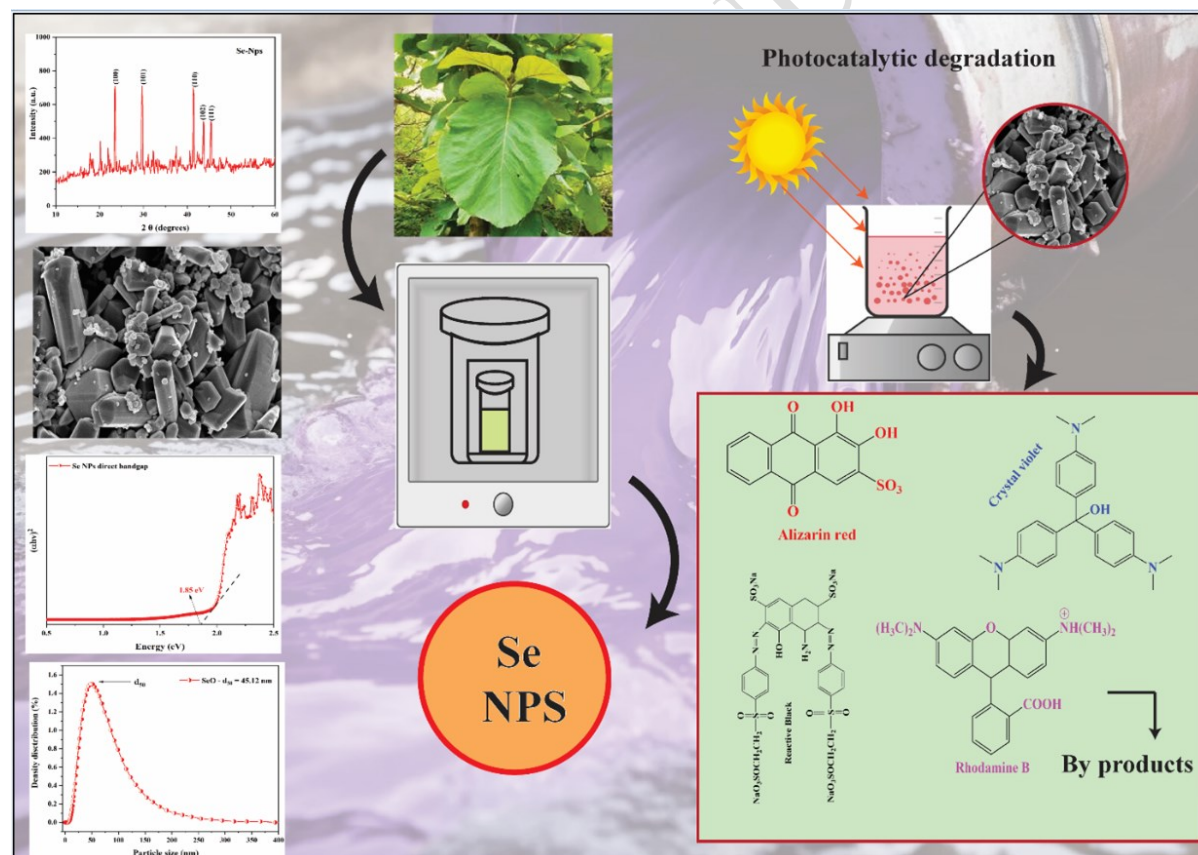
Abstract

This study synthesizes selenium nanoparticles (Se NPs) using a green approach, utilizing *Tectona grandis* leaf extract in a hydrothermal method. The X-ray diffraction (XRD) analysis provided

highly crystalline particles with a trigonal crystal structure, indicative of the well-defined nature of the synthesized Se NPs. Particle size analysis (PSA) results demonstrated a average particle size of 45 nm, further supporting the nano-sized characteristics of the particles. Field emission scanning electron microscopy (FESEM) results exhibited a hexagonal close-packed structure, providing valuable insights into the morphology of the Se NPs. Optical band gap calculations using the Tauc plot method yielded a value of 1.85 eV, highlighting the semiconductor nature of the synthesized Se NPs. Rhodamine B exhibited the highest degradation efficiency among the dyes, reaching 96%. Furthermore, the stability of the Se NPs was evaluated through five consecutive cycles of photocatalytic degradation. Remarkably, the nanoparticles maintained stability, with only a marginal loss in degradation efficiency (after 5 cycles), affirming their potential as a stable and efficient nano photocatalyst for environmental remediation applications. This comprehensive investigation underscores the significance of green-synthesized Se NPs in advancing sustainable and effective photocatalytic processes.

1. Introduction

The textile industry is instrumental in fulfilling the worldwide demand for clothing and fabric products. Nevertheless, the widespread utilization of synthetic dyes in textile processing has given rise to environmental apprehensions stemming from the release of colored wastewater. These effluents not only contribute to aesthetic pollution but also have the potential to induce eutrophication and generate byproducts that may pose hazards to the environment (Phugare *et al.,* 2011). The water generated during azo dyeing operations, on the other hand, has a large molecular weight and a complicated structure, limiting its ability to breakdown (Chung *et al.,* 2016). This characteristic gives rise to distinct ecological challenges. Such effluents elevate water turbidity and impede sunlight penetration into aquatic bodies, disrupting biodiversity development. Industrial dyes, designed to withstand harsh conditions such as sunlight, moisture, chemical degradation, and corrosion, possess properties that prevent their natural detachment or decomposition into non-toxic components. Traditional wastewater treatment methods such as flocculation, coagulation, reverse osmosis, eletrocoagulation, ion exchange and sedimentation have proven ineffective in addressing the challenges posed by the chemical stability of synthetic textile dyes, prompting the exploration of advanced and sustainable approaches (Verma *et al.,* 2012). However, the techniques mentioned above primarily involve extracting organic substances

from aqueous solutions into a distinct phase, often raising concerns about the contamination of this secondary phase. Due to the need to replace adsorbents and process solid materials further, the overall cost of operations would increase. As an advanced oxidation process, photocatalysis shows considerable potential by utilizing light-induced reactions to degrade organic compounds (Alinsafi *et al.,* 2005). This method distinguishes itself for its capability to completely mineralize targeted pollutants, providing a more comprehensive purification of water resources. In contrast to traditional techniques like adsorption on activated carbon or chemical coagulation, photocatalysis circumvents the transfer of dye molecules from one phase to another, reducing the likelihood of secondary pollution. The photocatalytic degradation process directly focuses on the degradation of dye molecules, causing the breakdown of complex structures into environmentally benign byproducts. The selection of catalyst material is crucial in influencing the effectiveness of photocatalytic reactions (Barnaby *et al.,* 2011).

Several nanomaterials such as ZnO, TiO$_2$, La$_2$O3, CdS, NiO, MnO$_2$, and MgO have recently been assessed for their catalytic activity on the degradation of textile dyes in recent years (Dotto *et al.,* 2019). Selenium (Se) is one of the most important critical elements for every biological species since it is essential for the biological production of necessary selenoenzymes (Naushad *et al.,* 2019). Selenium nanoparticles (SeNPs) are fewer toxic and more biocompatible than their counterparts, selenium, selenate, and selenite. SeNPs have significantly less severe, temporary, and sub-chronic toxicity than selenite. SeNPs have many biological functions and clinical actions, such as antioxidant, antiprotozoal, anticancer, and antibacterial qualities (Sahinkaya *et al.,* 2019). Furthermore, their improved semiconducting, photo conducting, photoelectrical, and catalytic capabilities attract substantial attention in optics and electronics—these qualities position SeNPs as suitable candidates for various industrial and medicinal applications. Se NPs are synthesized through diverse chemical, physical, and biological methods (Aragaw *et al.,* 2023). In this study, with a primary focus on the practical application of degrading textile dyes, it becomes crucial to precisely adjust the morphology optical band gap and ensure the biocompatibility of Selenium nanoparticles (Se NPs). As a result, our objective is to produce Se NPs employing *Tectona grandis* (Teak) leaf extract as both a reducing and stabilizing agent, employing the hydrothermal method. Teak plants, belonging to the Verbenaceae family, are a source of anthocyanin pigments that can serve as natural dyes (Viswanathan *et al.,* 2018). Teak leaves contain a variety of bioactive

phytochemicals, including anthraquinones, deoxy lapachol, naphthoquinone, phenolic acids, tannic acids, flavonoids, saponins, rutin, and ellagic acids. These widely present phytochemicals can potentially enhance the surface properties of nanoparticles. Moreover, these leaves exhibit unique features such as anti-erythrogenic, antithetic, anti-ulcerogenic, anti-viral, anti-diuretic, antimicrobial, and anti-inflammatory activities and can treat low blood sugar levels. Hydrothermal methods involve high-temperature and high-pressure aqueous environments, providing a unique platform for the controlled growth and development of nanoparticles. In the context of selenium nanoparticles (Se NPs) synthesized for photocatalytic applications, hydrothermal is crucial in tailoring the resulting nanomaterials' size, morphology, and crystalline structure. The controlled reaction conditions within the hydrothermal environment allow for precise modulation of parameters including time of reaction, temperature and pressure control influencing the nucleation and growth kinetics of the nanoparticles.

Furthermore, in this investigation, the Selenium nanoparticles (Se NPs) prepared through a novel green synthesis approach are subjected to characterization using X-ray Diffraction (XRD), Fourier Transform Infrared spectroscopy (FTIR), Field Emission Scanning Electron Microscope (FESEM), Dynamic Light Scattering (DLS), Energy Dispersive X-ray analysis (EDX), and UV-Vis spectroscopy. The purpose of these investigations is to investigate the physicochemical characteristics of the produced Se NPs. Furthermore, the Se NPs are tested for efficiency against various cationic and anionic dyes in order to determine their practical applicability in degrading textile colors.

2. Experimental details

2.1. Materials and Methods

Sodium selenate (Na_2SeO_3) (99.9 % purity) is a precursor material to synthesize Se NPs. The leaves of Tectona grandis were gathered from nearby fields in Tiruchengode, Tamilnadu, India. This study utilized ethanol (99.9 % purity) and Double distilled (DD) water as solvents. All chemicals employed in this study are purchased from Loba Chemie (India). *Tectona grandis* leaves were gathered and cleaned with deionized water to remove the attached debris. Subsequently, the washed leaves were air-dried in the shade for 4 days and then finely powdered using a household mixer. Employing a magnetic stirrer, 5 grams of the powdered leaves were macerated in 100 mL of DD water with continuous stirring at 70°C for 8 hours. The resulting leaf extract was allowed

to cool to room temperature. The filtration process utilized Whatman No.1 filter paper, and a suction pump aided in separating the extracts (Boroumand *et al.,* 2019). The obtained *Tectona grandis* leaf extract solution was the reducing agent for synthesizing Selenium nanoparticles. The plant extract prepared was heated to 60°C with continuous stirring. Subsequently, a stoichiometric weight of 0.1 M Sodium selenate (Na_2SeO_3) was introduced to the solution, and stirred continuously for 30 minutes. After achieving homogenous dissolution, the solution was moved to a Teflon-lined autoclave fitted in a stainless steel container. For 9 hours, this configuration was placed in a hot air oven set to 180°C. The solution was collected and centrifuged at 4000 rpm after cooling to ambient temperature. The settled sediment underwent several washes with ethanol and water to eliminate precursor compounds. For 10 hours, the slurry was dried in a hot-air oven set at 60°C. The obtained dried powder was then annealed for 1 hour at 300°C. The Selenium nanoparticles created in this procedure were dubbed "Se NPs." Figure 1 displays a simplified graphical representation of Se Nps synthesis (Tugarova *et al.,* 2018).
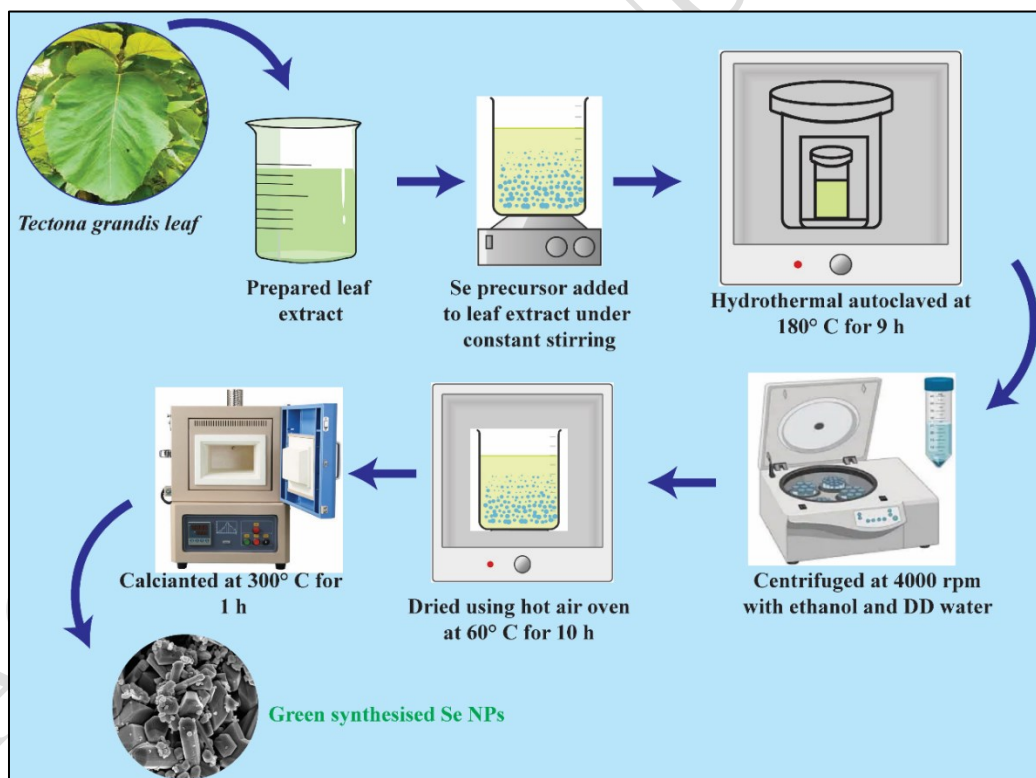

Figure 1. Green synthesis methodology of Se NPs

2.2. Characterization techniques

The synthesized Selenium nanoparticles (Se NPs) were subjected to comprehensive characterization using various analytical techniques to explicate their physicochemical properties.

X-ray Diffraction analysis (XRD; X'Pert PRO; PANalytical, Almelo, the Netherlands) with Cu anode at 40 kV and 30 mA was used to examine the crystalline structure of the Se NPs. The experiment was conducted in the 2θ range, from 20-80º, with a step size of 0.0170. was utilized to examine the crystalline structure of the Se NPs. This offers information on the nanoparticles' crystal size, shape, and orientation. To identify significant functional groups on the surface of the Se NPs, Fourier Transform Infrared Spectroscopy (FTIR) (Spectrum100; PerkinElmer, USA) was used. The FTIR was performed by employing KBr as background. This helps understand the chemical composition and potential biomolecules in the nanoparticles. The hydrodynamic size and distribution of Se NPs in solution were identified using the Dynamic light scattering technique (DLS) and a particle size analyzer (PSA) (Nanophox, Sympatec, Germany).

Field emission Scanning electron microscopy (FESEM) is used to analyze the shape, size distribution, and indepth morphology of nanoparticles. Additionally, energy dispersive spectroscopy (EDAX) (X Flash 7, Bruker) was used to analyze the chemical and elemental composition of the Se NPs. UV-Vis spectroscopy (Cary 8454, Agilent Technologies, Singapore) was used to examine the optical properties of the Se NPs. The absorption spectra reveal information about the band gap and electronic transitions, offering insights into the potential applications of the nanoparticles. The photocatalytic experiment was evaluated with various cationic and anionic dyes, and the decrease in absorbance was assessed using UV-Vis spectroscopy.

2.3. Photocatalytic experiment methadology

The photocatalytic dye degradation performance of prepared Se NPs was analyzed with various textile dyes used in the textile industry, such as Alizarin red (AR), Crystal violet (CV), Reactive Black (RB), and Rhodamine B (RhB). The experiments were performed under sunlight irradiation to mimic real-world conditions (Dwivedi *et al.,* 2011). A 15-ppm dye solution was prepared for each dye by dissolving 15 mg/L of dye in 1 L of DD water. The dye solution was initially irradiated to evaluate the degradation without a catalyst. To achieve catalyst-dye equilibrium, the synthesized Se NPs at a concentration of 5 ppm was used as the catalyst, and the mixture was agitated in a dark environment. Then, the solutions were irradiated under mid-day sunlight to attain maximum light intensity. The total duration of the experiment was set to 90 minutes, during which absorbance readings were recorded at 10-minute intervals. The absorbance measurements were taken at the maximum intensities observed for each dye, ensuring accurate monitoring of the photocatalytic

degradation process. The photocatalytic degradation efficiency of prepared Se NPs was evaluated through the following equation (Reza *et al.,* 2017).

$$Degradation\ efficiency\ (\%) = \left(1 - \frac{C}{C_0}\right) \times 100$$

3. Results and discussion

3.1. X-ray Diffraction

As depicted in Figure 2, the XRD pattern of prepared Se NPs has sharp peaks at the 2θ positions 23.5, 29.7, 41.4, 43.7, and 45.5. The observed peak position correlates with the crystalline planes (100), (101), (110), (102) and (111) respectively. The estimated lattice parameters a=4.362 Å and c=4.951 Å resemble to the trigonal crystal structure of Se NPs that corresponds with the JCPDS card No: 06-0362 [31,32]. The sharp peaks observed for prepared Se NPs suggest the high crystallinity of the nanoparticles. Further, the following Debye Scherrer equation was employed to evaluate the average crystalline size for prepared Se NPs (Bhatia *et al.,* 2017).

$$D\ (cryallite\ size) = \frac{K\lambda}{\beta\ cos\theta}$$

Where, the diffraction angle is θ, the full width at half maximum is β, the wavelength of the X-ray radiation is λ, and the grain size is D. The constant K is assumed to be 0.94. As shown in Table 1, the average crystalline size of prepared Se Nps is 30.02 nm. The lattice parameters and microstrain percentage calculated from XRD data are also shown in Table 1.

Table 1. Structural parameters obtained from XRD data of prepared Se NPs

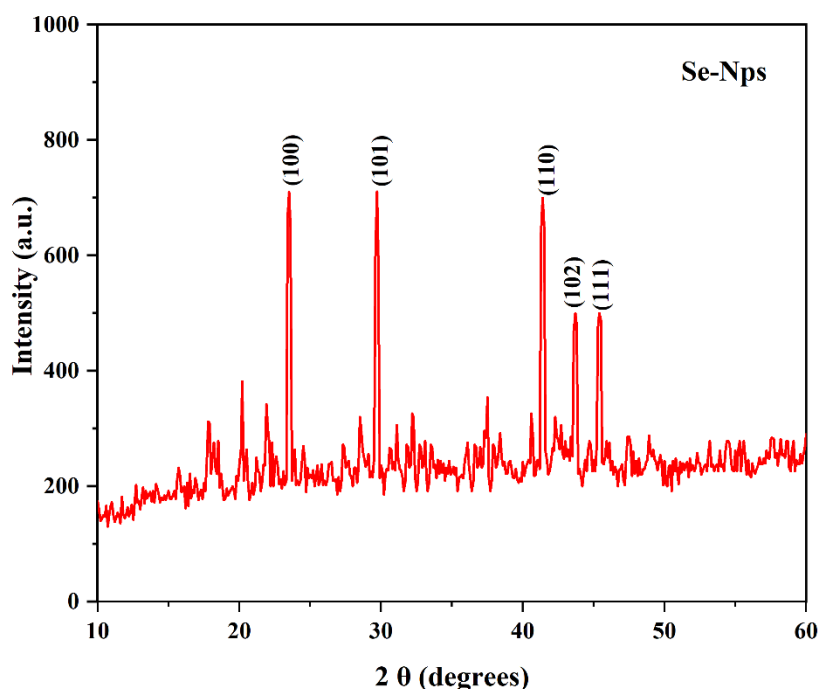| NPs	2 θ Position	hkl values	Crystallite size (nm)	Average crystalline size (nm)	Lattice parameters (Å)	Micro strain (%)
Se NPs	23.5	(100)	15.7	30.02	a=4.362Å & c= 4.951 Å	0.420317
	29.7	(101)	32.3			0.408375
	41.4	(110)	33.1			0.370231
	43.7	(102)	33.9			0.359178
	45.5	(111)	35.1			0.29578

Figure 2. XRD pattern of prepared Se NPs

3.2. Fourier Transform Infrared spectroscopy

The prepared selenium nanoparticles (Se NPs) FTIR spectrum exhibits distinctive peaks that provide insights into the chemical composition and functional groups present in the nanoparticles, as seen in Figure 3. Notably, a broad and prominent peak in the region around 3300 cm^{-1} is observed, corresponding to the stretching vibrations of hydroxyl groups (OH) (El-Sayed *et al.,* 2020). This observation suggests the adsorption of water molecules, either by the samples or the KBr used as a background. Peaks in the 2800-3000 cm^{-1} region indicate C-H stretching vibrations (Fardsadegh *et al.,* 2019). These vibrations are characteristic of organic compounds with aliphatic hydrocarbon chains. Aliphatic C-H bonds suggest the involvement of compounds such as alkanes or alkenes in the green synthesis process. Furthermore, the FTIR spectrum displays several distinctive peaks linked to phytochemicals extracted from the leaf extract of Tectona grandis. Carbonyl (C=O) stretching vibrations are indicated by peaks in the 1600–1700 cm^{-3} range, which may indicate the presence of ketones, aldehydes, or acids with carboxylic groups. Furthermore, peaks in the 1400-1500 cm^{-1} range correlates to the bending vibrations of methyl and methylene groups, common in organic molecules. The identified peaks in the FTIR spectrum affirm the involvement of phytochemicals from *Tectona grandis* leaf extract in the reduction and stabilization of selenium nanoparticles (Tripathi *et al.,* 2020).
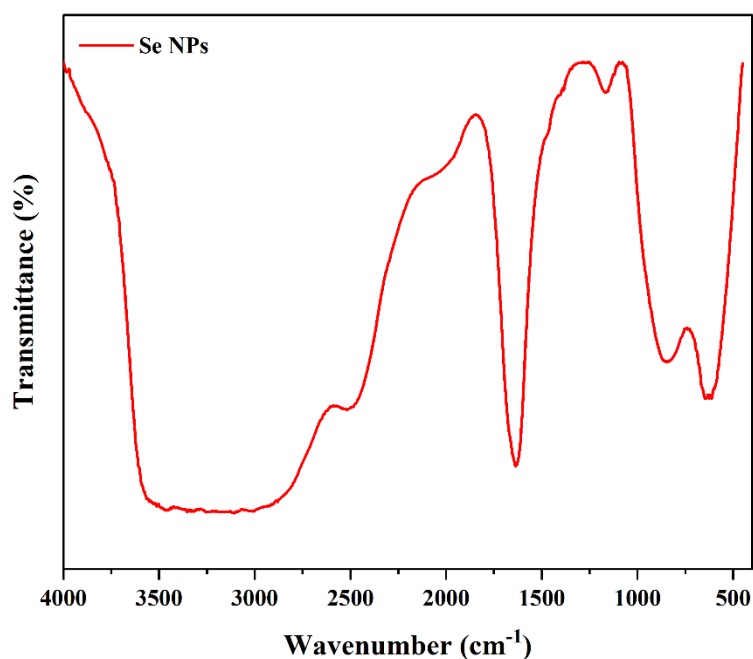
Figure 3. Functional groups present in Se NPs

3.3. Particle size analysis

 The dynamic light scattering approach was utilized to evaluate the particle size of the synthesized selenium nanoparticles (Se NPs). As depicted in Figure 4, the average diameter of the nanoparticles is determined to be 45.12 nm. Furthermore, the D_{10} value, representing the diameter below which 10% of the particles reside, is measured at 4 nm. This suggests the presence of a fraction of relatively small nanoparticles, each with a size less than 4 nm. Conversely, the D_{90} value, indicating the diameter below which 90% of the particles are found, is determined to be 150 nm. This underscores the prevalence of nano-sized particles in the sample, with the majority having a size of less than 150 nm. The phytochemicals found in *Tectona grandis* leaves, including polyphenols, flavonoids, and terpenoids, act as effective reducing agents, facilitating the formation of Se NPs with extremely small particles (Shedbalkar *et al.,* 2016). Furthermore, an important factor affecting the characteristics and possible uses of the nanoparticles is the relationship between the synthesis technique and particle size. In this context, the hydrothermal process, renowned for its controlled and uniform growth conditions, contributes to achieving a relatively narrow size distribution (Sadiq *et al.,* 2021).
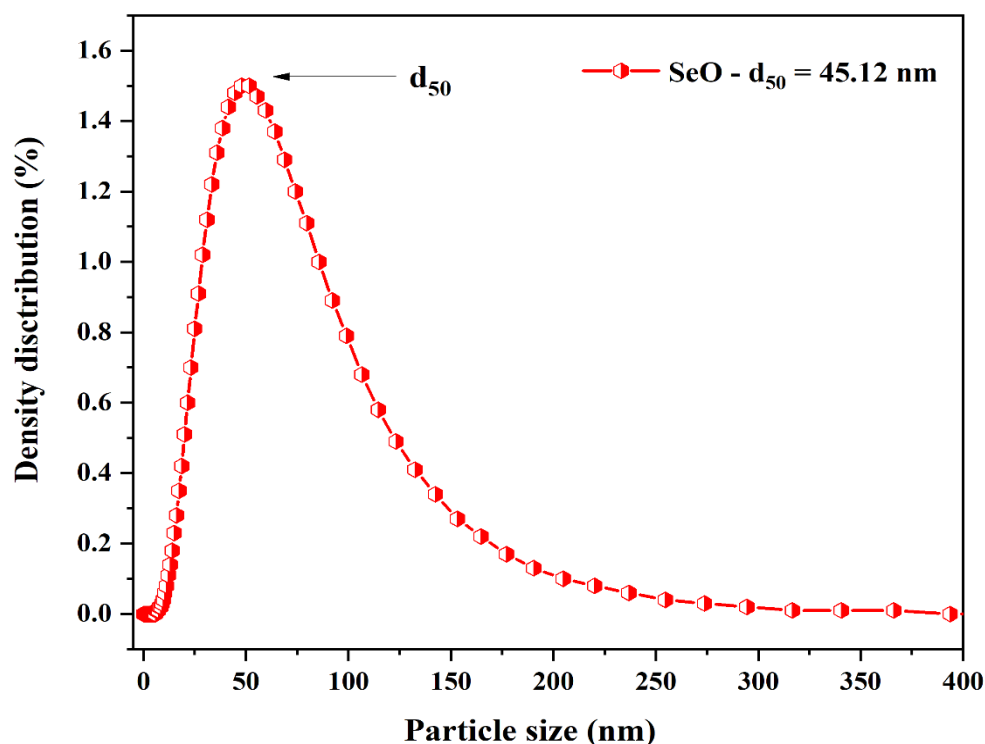
9

Figure 4. Particle size distribution of Se NPs

3.4. Field Emission Scanning Electron Microscope and Energy-Dispersive X-ray analysis

The field emission scanning electron microscopy (FESEM) analysis provides valuable insights into the morphology of prepared Se NPs. As depicted in Figure 5, the FESEM images reveal distinct hexagonal closely packed structures, indicative of the well-organized arrangement of Se NPs. The *Tectona grandis* leaf extract, rich in phytochemicals, acts as a natural reducing agent, facilitating the reduction and stabilization of selenium ions to form nanoparticles. The hydrothermal conditions, characterized by elevated temperature and pressure, show a pivotal role in directing the growth and morphology of the Se NPs. The synergistic effects between selenium ions and the bioactive complexes in the leaf extract contribute to the observed hexagonal closely packed structures (Tripathi *et al.,* 2020). The hexagonal, closely packed structures exhibit superior light absorption and scattering properties, allowing efficient utilization of incident photons during photocatalysis. Additionally, the intimate contact between Se NPs and the surrounding medium, facilitated by the specific morphology, promotes effective charge transfer processes crucial for photocatalytic reactions.
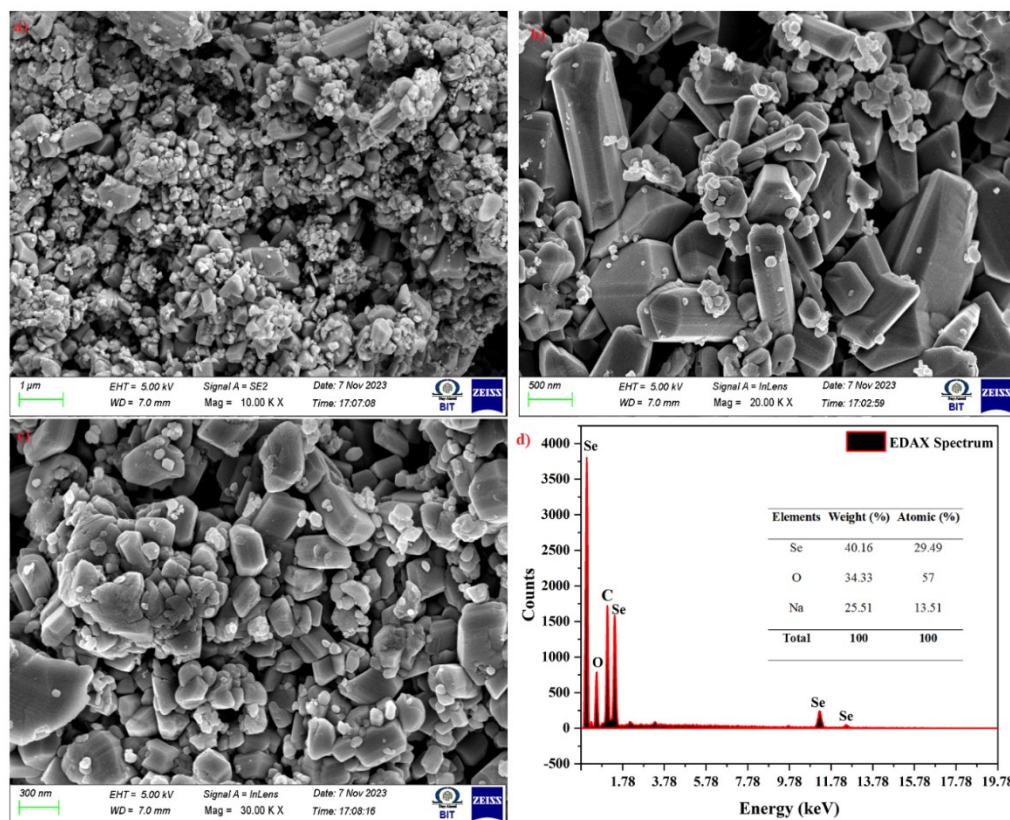
Figure 5. FESEM image of prepared Se NPs (a, b, and c) and EDAX analysis (d)

Additionally, the energy-dispersive X-ray (EDX) spectrum obtained during the FESEM analysis further corroborates the elemental composition of the prepared Se NPs. The peaks in the spectrum correspond to the energy level of selenium (Se), Carbon (C), and oxygen (O), confirming the presence of mentioned elements in the synthesized nanoparticles (Sadiq *et al.,* 2021). The weight percentage and atomic percentage of the Selenium element demonstrate the successful creation of Se NPs using Tectona grandis leaf extract as the stabilization and reduction agent in a green synthesis approach. The incorporation of carbon can be attributed to the biological components in the *Tectona grandis* leaf extract, which may contribute to the stabilizing and capping of the Se NPs.
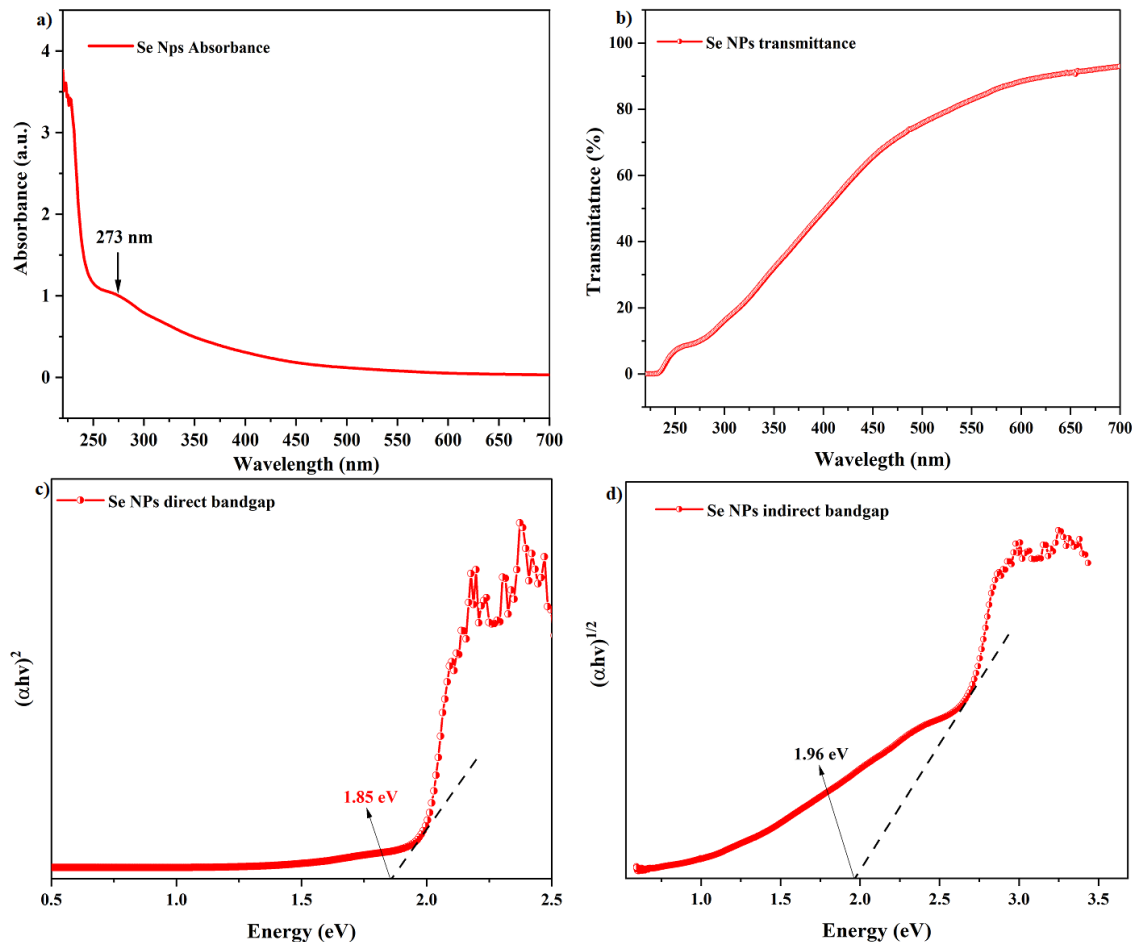
Figure 6. UV-Vis analysis of prepared Se NPs a) Absorbance, b) Transmittance, c) Direct band gap, and d) Indirect band gap

3.5. UV-Vis spectroscopy

The absorbance characteristics of selenium nanoparticles (Se NPs) were thoroughly investigated through ultraviolet-visible (UV-Vis) spectroscopy, providing crucial insights into their optical behavior, as seen in Figure 6. The absorption spectrum of Se NPs exhibited a distinct peak at 273 nm, signifying the absorption of ultraviolet light by the nanoparticles. The absorption spectrum observed for prepared Se NPs correlates closely with the earlier reports (Zhang *et al.,* 2005). The transmittance spectrum calculated from the absorption data is provided in Figure 6(b). To gain insights into the band structure, the band gap of Se NPs was estimated by employing the Tauc plot equation (Shedbalkar *et al.,* 2016).

$$(\alpha h v)^n = B\left(h v - E_g\right)$$

Where hv denotes photon energy, α denotes the absorption coefficient, C denotes the constant, and n, based on whether the transition is direct or indirect, is represented, the direct band gap is determined as the energy difference between the absorption edge and the extrapolated baseline, was found to be 1.85 eV. Simultaneously, the indirect band gap, calculated through the onset of the absorption curve, was measured at 1.96 eV. These band gap values are crucial parameters influencing the photocatalytic activity of Se NPs. The observed values align with the semiconductor nature of selenium, emphasizing its potential as an efficient photocatalyst in various applications, including environmental remediation and light-induced catalysis.

3.6. Photocatalytic activity

The prepared Se NPs' photocatalytic performance demonstrated significant AR, CV, RB, and RhB dyes' decolorization and decreased dye compounds' adsorption intensity, as shown in Figure 7. Over a consistent 90-minute duration, Se NPs exhibited notable degradation efficiencies of 86.87%, 91.16%, 84.7%, and 94.93% for AR, CV, RB, and RhB dyes, respectively. The Se NPs displayed significant potential in degrading the employed model dyes, with a notably higher degradation efficiency observed for cationic dyes (CV & RhB) compared to anionic dyes (AR and RB). The negative surface charge of the produced NPs facilitates the adsorption of positively charged cationic dye molecules, resulting in improved degradation against cationic dyes. Furthermore, the degradation kinetics of Se NPs were assessed using the Pseudo First Order degradation kinetic model, expressed by the following equation (Tugarova *et al.,* 2017).

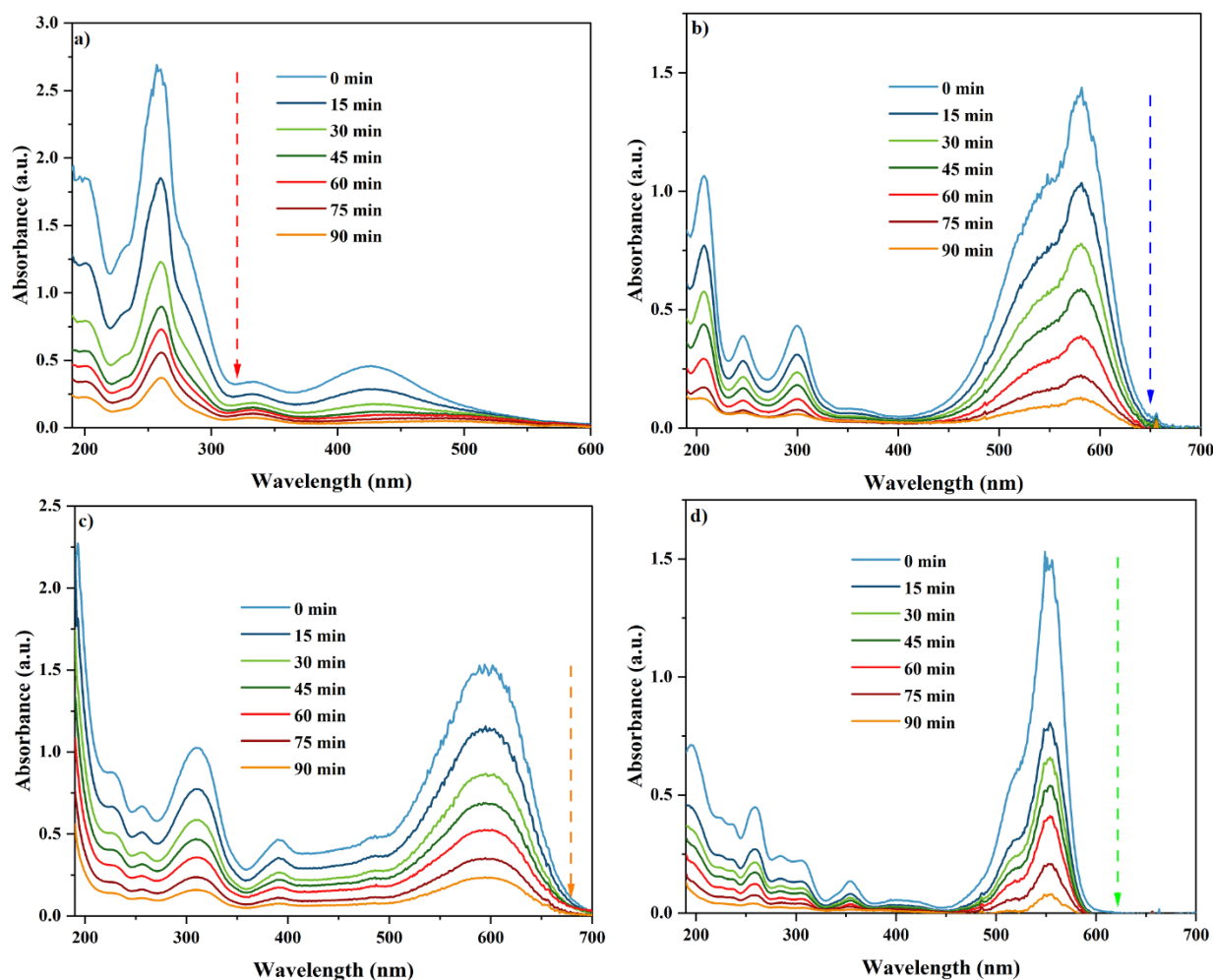$$\ln\left(\frac{C}{C_0}\right) = kt$$

Figure 7. Photocatalytic activity of Se NPs towards a) AR, b) CV, c) RB, and d) RhB model dyes

Where the initial and time-dependent concentrations of dye compounds are C and C_0, k represents the kinetic rates constant, and t represents the time. The C/C_0 curves for dye compounds and the corresponding linear fit curves are provided in Figure 8. The obtained kinetic degradation rate values shown in Table 2 indicate a gradual degradation of dye compounds in the presence of Se NPs, and the high R^2 values signify an excellent linear fit of the first-order degradation model. These findings underscore the efficacy of Se NPs in the photocatalytic degradation of textile dyes. Additionally, the average degradation rate of cationic dyes is 1.38 times higher than that of anionic dyes, highlighting the selective efficiency of Se NPs in the degradation process. As indicated in Table 3, the synthesized Se nanoparticles' degradation efficiency is notably higher than previously

14

green-synthesized nanomaterials. The prepared Se nanoparticles exhibit efficient performance even at lower catalyst concentrations.
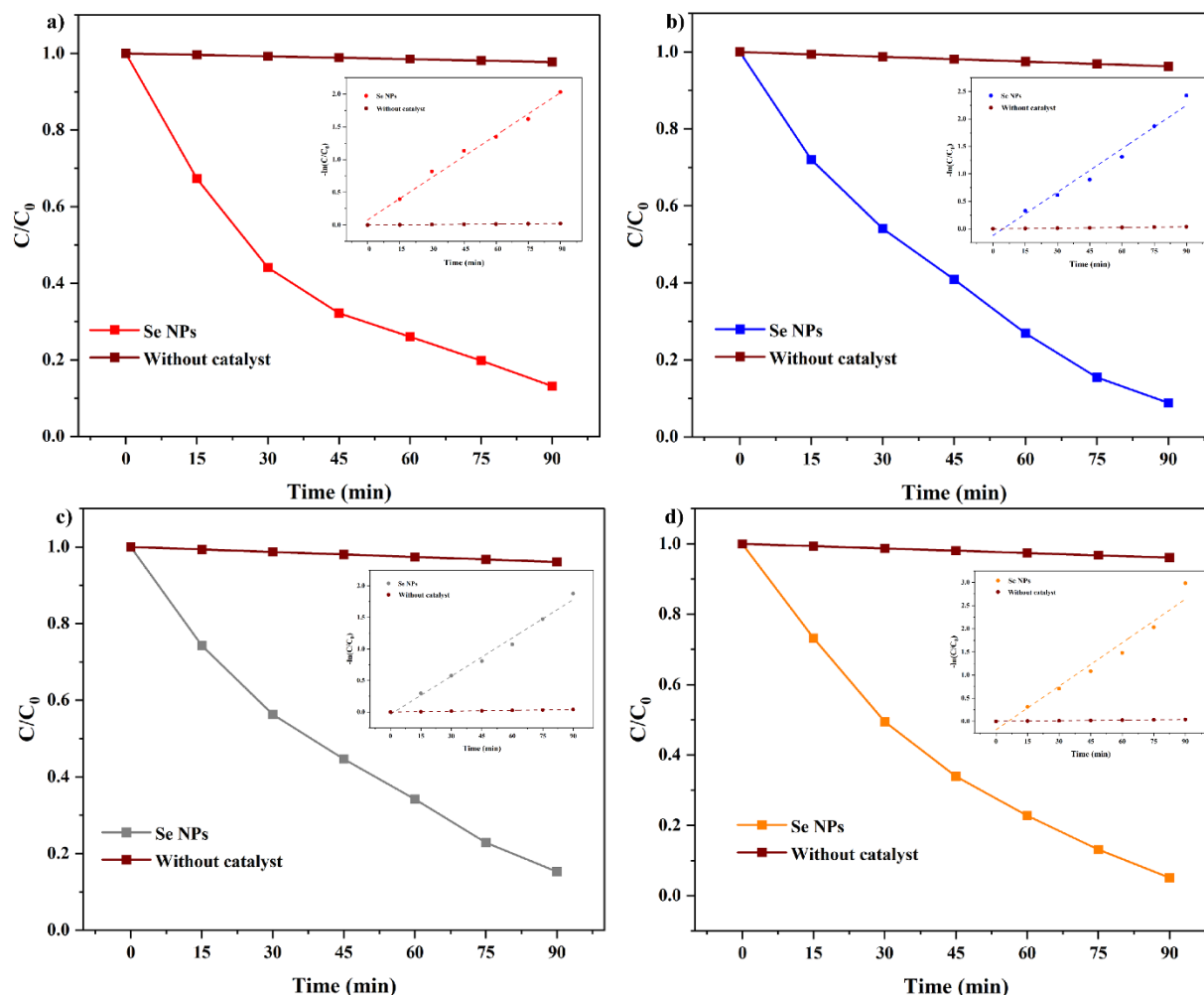

Figure 8. C/C0 curve fitted with pseudo-first-order degradation kinetic of Se NPs towards a) AR, b) CV, c) RB, and d) RhB model dyes

3.7. Degradation mechanism

The degradation of model dyes through prepared Se NPs could occur in various ways, such as photocatalytic degradation, surface charge adsorption, and facilitating the role of attached phytochemicals, as seen in Figure 9. Sunlight initially irradiates electrons from the valence region to the conduction region of Se NPs during photocatalytic degradation. A photon's energy level (hv) upon absorption is equal to or greater than the catalyst's band gap.

Table 2. Obtained degradation and kinetic values for prepared Se NPs towards model dyes

15

NPs	Dyes	Degradation efficiency (%)	Without catalyst Kinetic rate (min⁻¹)	With catalyst Kinetic rate (min⁻¹)	R^2
Se	Alizarin red	86.87	2.4×10^{-4}	2.15×10^{-2}	0.977
	Crystal violet	91.16	4.2×10^{-4}	2.63×10^{-2}	0.977
	Reactive black	84.7	4.4×10^{-4}	2.02×10^{-2}	0.989
	Rhodamine B	94.93	4.1×10^{-4}	3.13×10^{-2}	0.972

This energy excites the semiconductor, creating a hole in the valence band (h_{VB}^+) and generating an electron-hole pair (e^-/h^+). This involves the formation of simultaneous electron and hole generation within the catalyst material (equation 1). Due to photon absorption, the holes formed in the valence band react with water, forming potent OH˙ radicals (equation 2). These OH radicals forming on the irradiation semiconductor's surface behave as powerful oxidizing agents. They can attack adsorbed organic molecules and those close to the catalytic surface. Organic pollutants are mineralized due to this non-selective oxidation, depending on their molecular structure and stability. Furthermore, OH radicals can kill germs, increasing the entire cleaning process. An electron from the conduction band simultaneously interacts with oxygen, generating an anionic superoxide radical. This superoxide ion participates in subsequent oxidation incidents and is critical in avoiding electron and hole recombination, preserving overall electron neutrality within the catalyst molecule. Protonation of the produced anionic superoxide radical (O_2) results in the creation of a hydroperoxyl radical (HO_2), which then changes into hydrogen peroxide (H_2O_2) (equation 3). H_2O_2 molecules can split into extremely reactive hydroxyl radicals (OH). These hydroxyl radicals, in turn, react with dye substances, triggering an oxidation process that degrades the colors' chemical structure. (equation 4).

$$(1) \quad Se\ NPs + h\upsilon \rightarrow h_{VB}^+ + e_{CB}^-$$
$$(2) \quad H_2O + h_{VB}^+ \rightarrow H^+ + \ ^\cdot OH$$
$$(3) \quad O_2 + e_{CB}^- \rightarrow O_2^-$$
$$(4) \quad Dye\ molecules + OH + O_2^- \rightarrow By\ products + CO_2 + H_2O$$
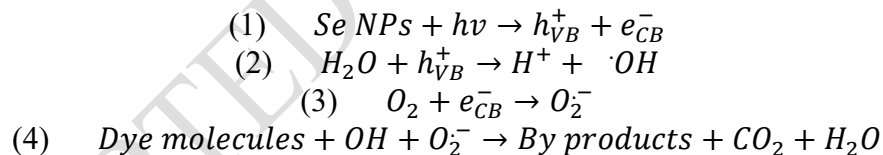
The second process that aids in the breakdown of dyes involves surface charge adsorption. The selective adsorption of cationic dyes such as Crystal violet and Rhodamine B is observed during degradation. This selectivity can be attributed to the electrostatic interaction (attraction) between catalyst surface having negative charge and the positively charged dye substances. Additionally, the attachment of phytochemicals of *Tectona grandis* leaf with synthesized Se NPs plays a crucial role in dye molecule adsorption. Phytochemicals contribute to dye adsorption through various mechanisms. One such mechanism involves electrostatic attraction between phytochemicals and dye molecules.

Table 3. Comparative dye degradation analysis with earlier green synthesized NPs

S. No	Catalyst NPs	Green synthesis agent	Catalyst Conc.	Dye employed	Dye Conc.	Irradiation source	Irradiation time (min)	Degradation efficiency (%)	ref
1.	Se	*F. benghalensis*	100 mg/L	Methylene blue	10 mg/L	Visible light	40	57.63	[42]
2.	Fe$_3$O$_4$	*Carica papaya*	6 g/L	remazol yellow RR	50 mg/L	Sunlight	360	77	[43]
3.	ZnO	*Artocarpus heterophyllus*	10 mg/L	Rose Bengal	30 mg/L	Visible light	60	80	[44]
4.	SnO$_2$	*M.oliefera*	100 mg/L	Rhodamine B	1×10^{-5} M	Sunlight	90	86	[45]
5.	SnO$_2$	*chitosan*	~210 mg/L	Eriochrome Black T	6 mg/L	Visible light	270	77	[46]
6.	ZnO	*Syzygium Cumini*	50 mg/L	Methylene blue	20 mg/L	Sunlight	180	91.4	[47]
7.	ZnO	*Loquat seeds*	12 mg/L	Methylene blue	5 mg/L	UV light	200	~65	[48]
8.	CuO	*C.paniculatus*	10 mg/L	Methylene blue	10 mg/L	Sunlight	120	~90	[49]
9.	Se	*Tectona grandis*	5 ppm	Alizarin red	15 ppm	Sunlight	90	86.87	Present work
				Crystal violet	15 ppm	Sunlight	90	**91.16**	
				Reactive Black	15 ppm	Sunlight	90	84.87	
				Rhodamine B	15 ppm	Sunlight	90	**94.93**	

Phytochemicals possess functional groups like hydroxyl, carboxyl, and amino, enabling interactions with dye molecules through hydrogen bonding and electrostatic forces. Another mechanism involves the formation of complexes between phytochemicals and dye molecules. This occurs when phytochemicals chelate with dye molecules, creating a ring-like structure around the dye molecule, facilitating its removal from the solution.
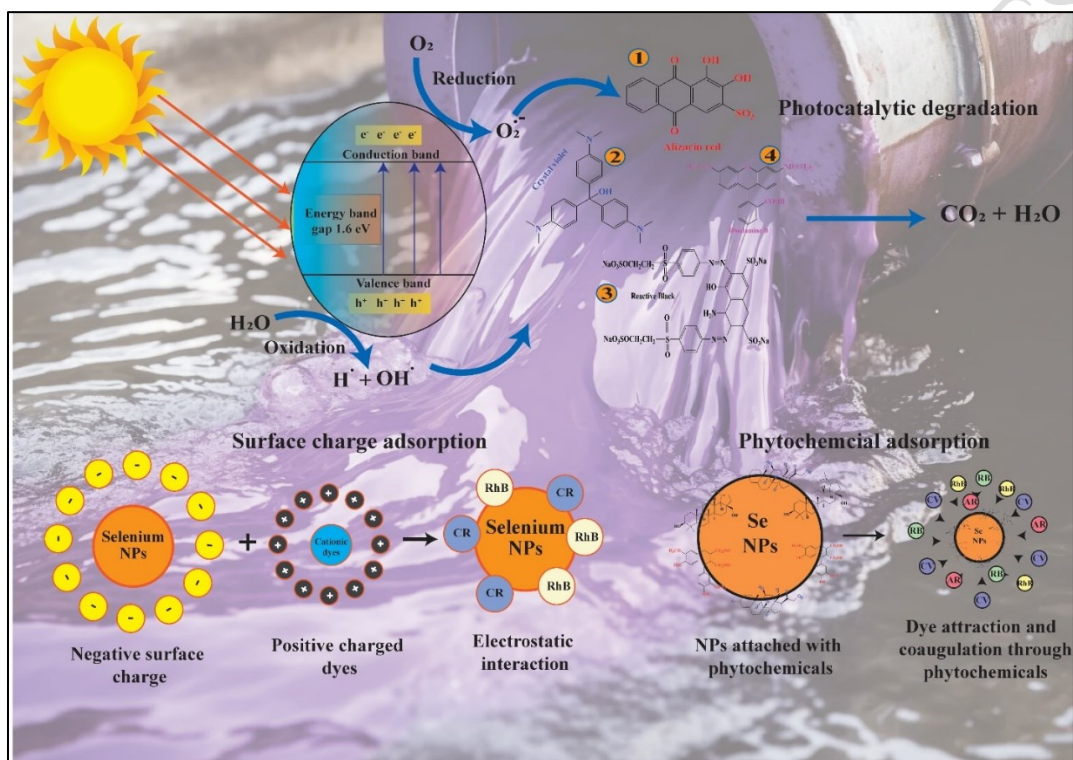

Figure 9. Degradation mechanism for prepared Se NPs

3.8. Cyclic stability

The cyclic stability assessment of Se nanoparticles (NPs) was conducted over five cycles to evaluate their performance in the degradation of AR, CV, RB, and RhB dyes. As illustrated in Figure 10, the degradation efficiency was monitored across consecutive cycles for each dye. The Se NPs demonstrated a steady and continuous degrading efficiency during the five cycles. Table 4 shows a slight drop in degradation efficiency across the dyes after the fifth cycle, ranging from 4% to 6.5%. This minimal loss in cyclic stability indicates the robustness and reliability of the prepared Se nanoparticles, highlighting their potential for repeated use on the degradation of textile dyes. The results suggest that the nanoparticles maintain their catalytic activity effectively over multiple

cycles, further emphasizing their stability and suitability for practical applications (Tugarova *et al.,* 2017).
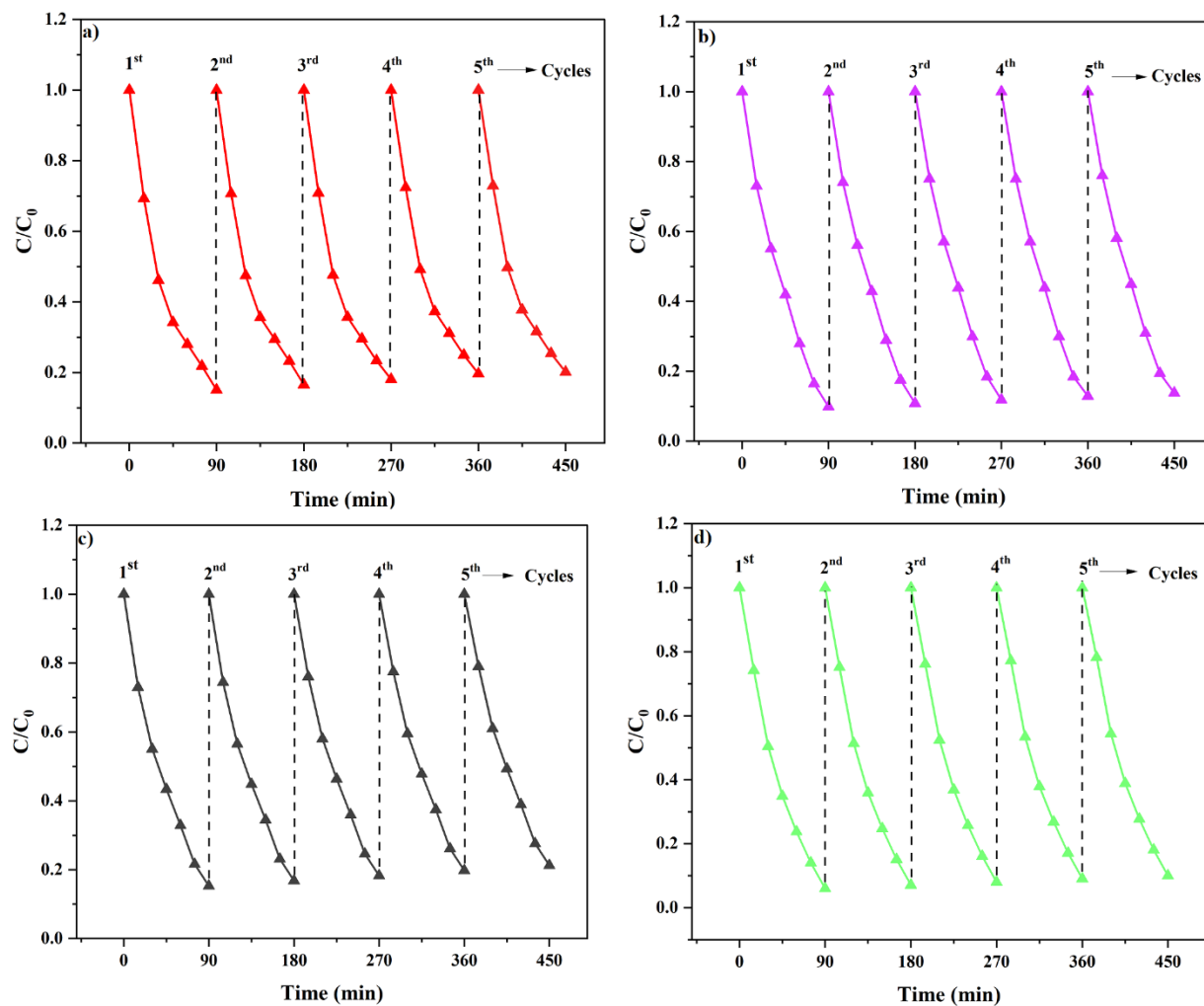

Figure 10. Cyclic stability of Se NPs towards a) AR, b) CV, c) RB, and d) RhB model dyes

Table 4. Cyclic stability of prepared Se NPs

NPs	Dye	Initial degradation (%)	Degradation after 5th cycle (%)	Efficiency loss (%)
	Alizarin red	86.87	**81.07**	**5.8**
Se	Crystal violet	91.16	**86.95**	**4.21**
	Reactive black	84.7	**78.37**	**6.33**
	Rhodamine B	94.93	**90.85**	**4.08**

4. Conclusion

In conclusion, this study successfully demonstrated the green synthesis of selenium nanoparticles (Se NPs) through a hydrothermal method, utilizing *Tectona grandis* leaf extract. The photocatalytic dye degradation performance of the Se NPs was assessed for the efficienct degradation of various cationic and anionic dyes under sunlight irradiation. Notably, the Se NPs showed remarkable efficacy in degrading cationic dyes, with Rhodamine B achieving an exceptionally high degradation efficiency of 96%. This superior performance can be attributed to the electrostatic surface charge interactions between the nanoparticles and cationic dye molecules. Crucially, the Se NPs exhibited stability over multiple photocatalytic cycles, with only a minor loss in degradation efficiency after five cycles. This exceptional stability underscores the potential practical application of these nanoparticles in sustainable and long-term environmental remediation processes. The green-synthesized Se NPs offer a promising avenue for developing efficient and eco-friendly nanomaterials for photocatalytic applications. The successful integration of a green synthesis approach and the notable photocatalytic performance and stability position these Se NPs as valuable candidates for future environmental remediation strategies. The results of this investigation add to the expanding corpus of information about environmentally friendly nanomaterials and their potential uses in solving environmental problems.

References

Alinsafi A., Khemis M., Pons M.N., Leclerc J.P., Yaacoubi A., Benhammou A. and Nejmeddine A. (2005). Electro-Coagulation of Reactive Textile Dyes and Textile Wastewater, *Chemical Engineering and Processing: Process Intensification*, **44,** 461–470.

Aragaw T.A. and Bogale F.M. (2023). Role of Coagulation/Flocculation as a Pretreatment Option to Reduce Colloidal/Bio-Colloidal Fouling in Tertiary Filtration of Textile Wastewater: A Review and Future Outlooks, *Frontiers in Environmental Science*, **11,** 1142227.

Barnaby S.N., Frayne S.H., Fath K.R. and Banerjee I.A. (2011). Growth of Se Nanoparticles on Kinetin Assemblies and Their Biocompatibility Studies, *Soft Mater*, **9,** 313–334.

Bhatia S. and Verma N. (2017). Photocatalytic Activity of ZnO Nanoparticles with Optimization of Defects, *Mater Res Bull*, **95,** 468–476.

Boroumand S., Safari M., Shaabani E., Shirzad M. and Faridi-Majidi R. (2019). Selenium Nanoparticles: Synthesis, Characterization and Study of Their Cytotoxicity, Antioxidant and Antibacterial Activity, *Materials Research Express*, **6,** 0850d8.

Chung K.T. and Azo D. (2016). Human Health: A Review, *Journal of Environmental Science and Health,* **34,** 233–261.

Dotto J., Fagundes-Klen M.R., Veit M.T., Palácio,S.M. and Bergamasco R. Performance of Different Coagulants in the Coagulation/Flocculation Process of Textile Wastewater, *Journal of Cleaner Production*, **208,** 656–665.

Dwivedi C., Shah C.P., Singh K., Kumar M. and Bajaj P.N. (2011). An Organic Acid-Induced Synthesis and Characterization of Selenium Nanoparticles, *Journal of Nanotechnology*, **1–6,** 651971.

El-Sayed E.S.R., Abdelhakim H.K. and Ahmed A.S. (2020). Solid-State Fermentation for Enhanced Production of Selenium Nanoparticles by Gamma-Irradiated Monascus Purpureus and Their Biological Evaluation and Photocatalytic Activities, *Bioprocess and Biosystems Engineering*, **43,** 797–809.

Fardsadegh B. and Jafarizadeh-Malmiri H. (2019). Aloe Vera Leaf Extract Mediated Green Synthesis of Selenium Nanoparticles and Assessment of Their In Vitro Antimicrobial Activity against Spoilage Fungi and Pathogenic Bacteria Strains, *Green Processing and Synthesis*, **8,** 399–407.

Naushad M., Alqadami A.A., Al-Kahtani A.A., Ahamad T., Awual M.R. and Tatarchuk T. (2019). Adsorption of Textile Dye Using Para-Aminobenzoic Acid Modified Activated Carbon: Kinetic and Equilibrium Studies, *Journal of Molecular Liquids*, **296,** 112075.

Phugare S.S., Kalyani D.C., Patil A.V. and Jadhav J.P. (2011). Textile Dye Degradation by Bacterial Consortium and Subsequent Toxicological Analysis of Dye and Dye Metabolites Using Cytotoxicity, Genotoxicity and Oxidative Stress Studies, *Journal of Hazardous Materials*, **186,** 713–723.

Reza K.M., Kurny A. and Gulshan F. (2017). Parameters Affecting the Photocatalytic Degradation of Dyes Using TiO_2: A Review, *Applied Water Science*, **7,** 1569–1578.

Wadhwani S.A., Shedbalkar U.U., Singh R. and Chopade, B.A. (2016). Biogenic Selenium Nanoparticles: Current Status and Future Prospects, *Applied Microbiology and Biotechnology*, **100,** 2555–2566.

Sadiq H., Sher F., Sehar S., Lima E.C., Zhang S., Iqbal H.M.N., Zafar F. and Nuhanovic M. (2021). Green Synthesis of ZnO Nanoparticles from Syzygium Cumini Leaves Extract with Robust Photocatalysis Applications, *Journal of Molecular Liquids*, **335,** 116567.

Sahinkaya E., Tuncman S., Koc I., Guner A.R., Ciftci S., Aygun A. and Sengul S. (2019). Performance of a Pilot-Scale Reverse Osmosis Process for Water Recovery from Biologically-Treated Textile Wastewater, *Journal of Environmental Management*, **249,** 109382.

Tripathi R.M., Hameed P., Rao R.P., Shrivastava N., Mittal J. and Mohapatra S. (2020). Biosynthesis of Highly Stable Fluorescent Selenium Nanoparticles and the Evaluation of Their Photocatalytic Degradation of Dye, *Bionanoscience*, **10,** 389–396.

Tugarova A.V. and Kamnev A.A. (2017). Proteins in Microbial Synthesis of Selenium Nanoparticles, *Talanta*, **174**, 539–547.

Tugarova A.V., Mamchenkova P.V., Dyatlova Y.A. and Kamnev A.A. (2018). FTIR and Raman Spectroscopic Studies of Selenium Nanoparticles Synthesised by the Bacterium Azospirillum Thiophilum, *Spectrochimica Acta, Part A: Molecular and Biomolecular Spectroscopy*, **192,** 458–463.

Verma A.K., Dash R.R. and Bhunia P. (2012). A Review on Chemical Coagulation/Flocculation Technologies for Removal of Colour from Textile Wastewaters, *Journal of Environmental Management*, **93,** 154–168.

Viswanathan B. (2018). Photocatalytic Degradation of Dyes: An Overview, *Current Catalysis*, **7,** 99–121.

Zhang J., Wang H., Yan X. and Zhang L. (2005). Comparison of Short-Term Toxicity between Nano-Se and Selenite in Mice, *Life Sciences*, **76,** 1099–1109.